

# JGR Atmospheres

## RESEARCH ARTICLE

10.1029/2023JD038542

### Key Points:

- First real-case assimilation of C-band phased-array radar clear-air data on convection initiation using Ensemble Kalman Filter
- Assimilating clear-air radial velocity plays a key role in successful forecast of convective initiation (CI)
- Assimilating clear-air radial velocity has the potential to accurately forecast CI with a lead time up to 20 min

### Correspondence to:

Y. Lu,  
[yinghuilu@nju.edu.cn](mailto:yinghuilu@nju.edu.cn)

### Citation:

Ming, J., Gong, P., Lu, Y., Zhao, K., Huang, H., Chen, X., et al. (2023). Impact of assimilating C-band phased-array radar data with EnKF on the forecast of convection initiation: A case study in Beijing, China. *Journal of Geophysical Research: Atmospheres*, 128, e2023JD038542. <https://doi.org/10.1029/2023JD038542>

Received 16 JAN 2023  
Accepted 13 NOV 2023

## Impact of Assimilating C-Band Phased-Array Radar Data With EnKF on the Forecast of Convection Initiation: A Case Study in Beijing, China

Jie Ming<sup>1,2</sup> , Peng Gong<sup>1,2</sup> , Yinghui Lu<sup>1,2</sup> , Kun Zhao<sup>1,2</sup> , Hao Huang<sup>1,2</sup> , Xingchao Chen<sup>3</sup> , Shuguang Wang<sup>1</sup>, and Qiang Zhang<sup>4</sup>

<sup>1</sup>Key Laboratory of Mesoscale Severe Weather/Ministry of Education, and School of Atmospheric Sciences, Nanjing University, Nanjing, China, <sup>2</sup>Key Laboratory of Radar Meteorology, China Meteorology Administration, Nanjing, China,

<sup>3</sup>Department of Meteorology and Atmosphere Science, Center for Advanced Data Assimilation and Predictability Techniques, The Pennsylvania State University, University Park, PA, USA, <sup>4</sup>Meteorology Center of North China Air Traffic Management Bureau, CAAC, Beijing, China

**Abstract** This study used a Weather Research and Forecasting (WRF)-based Ensemble Kalman Filter (EnKF) system to assimilate reflectivity ( $Z$ ) and radial velocity ( $V_r$ ) data in precipitating and clear-air regions from the Beijing Daxing International Airport C-band phased-array radar (C-PAR) to improve the forecasts of a convective initiation (CI) case occurred on 18 June 2020. The results showed that high-frequency assimilating the C-PAR  $V_r$  in clear-air region is conducive to increase the forecast lead time of CI by significantly improving the initial dynamic and thermodynamic fields, which creates a more accurate pre-CI environment. After assimilating the C-PAR clear-air  $V_r$ , the CI case can be accurately predicted with a 20 min forecast lead time in the best-case scenario. This is the first real-case study to demonstrate the benefits of assimilating high spatiotemporal resolution PAR clear-air radial velocity data for the CI process.

**Plain Language Summary** Convection initiation is the beginning stage of severe convective weather. Accurate prediction of its location and timing is very important for monitoring and early warning of severe convective weather. However, CI forecast is still a great challenge worldwide. The good news is that newly deployed phased-array radar (PAR) with high spatiotemporal resolution can capture the much needed small-scale information of the preconvective environment and the whole CI process. This study combines the new PAR observation and numerical weather prediction model through Ensemble Kalman Filter (EnKF), one of the most popular data assimilation techniques, to improve forecast of a CI event. With the improved data, we successfully forecast CI process mainly thanks to the PAR that help improved three-dimensional winds, temperature, and humidity analysis, particularly in the clear-air regions.

## 1. Introduction

Severe convective weather has always been the focal point in the weather forecast enterprise because of its destructive nature and dramatic occurrence. Convective initiation (CI), that air parcels first reach a level of free convection and then achieve and maintain positive buoyancy over a significant upward vertical excursion, is considered as the beginning of a severe convective weather event (Markowski et al., 2006). Previous studies typically defined CI as the radar reflectivity within a convective cloud first exceeding 35 dBZ (Abulikemu et al., 2016; Wilson & Schreiber, 1986). CI can be divided into two types: surface based or elevated. The surface-based CI is initialized by surface convergence lines during afternoon and early evening, while the elevated CI occurs during the night and early morning because of confluence at middle levels (between 900 and 600 hPa) or synoptic or mesoscale wind convergence (Wilson & Roberts, 2006). Many field experiments (Weckwerth & Parsons, 2006; Weckwerth et al., 2004, 2019; Wilson & Roberts, 2006) and modeling simulations (Abulikemu et al., 2016; Burghardt et al., 2014; Chen et al., 2017; Gebauer et al., 2018) have been conducted to study CI in recent years, leading to significant progresses in understanding of its mechanisms and improvement in numerical weather prediction of CI. It is now well recognized that the CI process is closely related to the multiscale interactions between convection and its large-scale environments (Burghardt et al., 2014; Johnson et al., 2015). So far, CI, as a critical stage of the whole convective life cycle, is often considered the least understood and worst forecasted stage due to its complex mechanisms (Lock & Houston, 2014), and is still a greatest challenge for weather forecasting (Clark et al., 2014).

Data assimilation, one of the most important techniques to improve numerical forecast capacity by improving the initial conditions of a numerical weather prediction model, aims to combine all available information to create the best estimate of the atmospheric state and uncertainty as accurately as possible (Meng & Zhang, 2011; Xiao et al., 2019). Many previous studies have devoted to studying the feasibility of assimilating traditional observation (e.g., surface and sounding observations) to improve CI forecast (Childs et al., 2006; Coniglio et al., 2019; Degelia et al., 2018; Gasperoni et al., 2018; Madaus & Hakim, 2017; Sobash & Stensrud, 2015). Childs et al. (2006) found assimilating the surface temperature and humidity observations can improve CI forecast due to better simulation of boundary layer moisture convergence through enhancing surface heat flux. Sobash and Stensrud (2015) assessed the impact of assimilating mesonet surface observations every 5 min in a dryline case. They found that the forecast of CI location and timing could be improved because the mesonet data can capture rapidly evolving mesoscale features and constrain model biases. Degelia et al. (2018) showed that assimilating in situ observations can increase low-level convergence and enhance buoyancy, leading to more accurate preconvective environment and mesoscale features analysis, and help successful CI forecasts especially in the evening. After carrying out a series of observing system simulation experiments, Madaus and Hakim (2017) confirmed that when surface observations have at least 4-km resolution, especially 1-km resolution, the storm-scale CI forecast becomes credible. Gasperoni et al. (2018) tested the impact of assimilating high spatiotemporal resolution nonconventional surface observations on timing and location of CI forecasts, and the result showed CI is successfully forecasted because the details in the dryline structure had been captured. Coniglio et al. (2019) found that assimilating Atmospheric Emitted Radiance Interferometer (AERI) and Doppler lidar (DL) wind profile observations have a positive impact on CI forecast.

However, traditional observation is still insufficient to provide enough high-frequency mesoscale and microscale information that is crucial for CI forecast due to resolution limitations in both time and space (Huang et al., 2022; Keclik et al., 2017). Keclik et al. (2017) assimilated midtropospheric to upper tropospheric, meso- $\alpha$ -scale to synoptic-scale Mesoscale Predictability Experiment dropsonde observations, and found that data assimilation is less helpful to improve CI forecast skills due to limited influence upon the lower-tropospheric processes. In contrast, Doppler radar is the most useful platform to monitor the fast-evolving convective-scale three-dimensional wind and thermodynamic fields in severe weather (Aksoy et al., 2009; Fabry & Meunier, 2020). The benefits of assimilating radar data to improve storm-scale analysis and forecast have been demonstrated and widely accepted in many previous studies (Rennie et al., 2011; Snyder & Zhang, 2003; Sun et al., 2014; Tong & Xue, 2005; Wang et al., 2022).

Although operational Doppler weather radar networks such as WSR-88D in United States and CINRAD WSR-98D in China are very helpful to severe weather monitoring and early warning, there is still a limitation for monitoring rapidly changing mesoscale and microscale weather processes since it takes 5–6 min to perform a volume scan. The low scanning rate is compounded by the incapability of probing lower troposphere and insensitivity on the detection of clear sky areas (Stratman et al., 2020; Zrnic' et al., 2007). In contrast, phased-array radar (PAR), which has electronic steering capability, can complete a volume scan in <2 min. Besides, PAR can flexibly switch its scanning strategy between clear-air and storm modes. Furthermore, PAR has excellent weak echo detection capability, which can realize early warning of severe weather. Therefore, PAR has advantages in monitoring fast-evolving mesoscale and microscale weather processes, and is more capable of capturing additional information in low altitudes compared with traditional weather radar (Huang et al., 2020; Lin et al., 2022; Supinie et al., 2017; Zrnic' et al., 2007). Huang et al. (2022) showed that the PAR clear-mode helps to capture at least part of the meso- $\gamma$ -scale to microscale features associated with CI. X. Zhang et al. (2022) selected the same case as our study and compared observations from PAR and CINRAD WSR-98D radar. Their result indicated that CINRAD WSR-98D radar failed to detect the weak echo until CI has already happened and convection has enhanced, 24 min delayed compared to first observation of CI from PAR.

The Ensemble Kalman Filter (EnKF) is one of the most popular data assimilation methods that using short-term ensemble forecasts to provide a flow-dependent estimate of background error covariance. EnKF was first developed by Evensen (1994) from the merger of Kalman filter theory and Monte Carlo estimation methods, and then first applied to atmospheric data assimilation by Houtekamer and Mitchell (1998). Many studies have shown the benefits of using EnKF to assimilate conventional or Doppler radar data (Snook et al., 2011; Snyder & Zhang, 2003; Sun et al., 2014; Tong & Xue, 2005; Wang et al., 2021). Miyoshi et al. (2016) developed “big data assimilation” system with high spatial resolution (100-m grid spacing) and high temporal resolution (refreshed every 30 s) assimilation of PAR data to forecast the evolution of a convective storm. The results proved the

concept that the assimilation of PAR helps the analysis of convective storms for the first time. Honda, Amemiya, Otsuka, Lien, et al. (2022) used a new data assimilation system named SCALE-LETKF developed by Lien et al. (2017) to assimilate PAR data every 30 s with high space resolution (500-m grid spacing) to forecast a real-time rapidly developing convective precipitation systems for the first time. Honda, Amemiya, Otsuka, Taylor, et al. (2022) elaborated details of analysis results of a CI process occurred in severe precipitation event, which proved the benefits of SCALE-LETKF system in assimilating PAR data to predict the rapid development of the small convective cell in a real-case study. Taylor et al. (2023) designed sensitivity studies to explore more suitable horizontal localization for forecasting precipitating convective systems by SCALE-LETKF and demonstrated the reason why spurious and intense convection developed. However, these studies only assimilate radar observations over precipitating areas, which may only provide limited information before CI. Assimilating radar observations over clear-air region obtained by high-sensitivity radars can provide more information of the pre-CI environment and thus may benefit CI forecast. Zrnic' et al. (2007) concluded that assimilating high spatiotemporal resolution clear-air boundary layer radar data may improve the timing and location of CI forecasts. Huang et al. (2022) revealed the potential benefit of assimilating synthetic PAR clear-air radial velocity observations on CI forecasts by a series of observing system simulation experiments (OSSEs). However, there is still a lack of real-case study on assimilating PAR data for CI forecast to the best of our knowledge.

This study will explore the impact of assimilating real PAR data especially V<sub>r</sub> in the clear-air region on CI forecasts using the Weather Research and Forecasting (WRF)-EnKF system originally developed by Meng and Zhang (2008a, 2008b). The rest of this paper is organized as follows: Section 2 documents the case overview, data description, and experimental design. The analysis results and forecasting results are discussed in Section 3. Summary and conclusions are given in Section 4.

## 2. Data and Methods

### 2.1. Case Overview and Data Description

The C-band phased-array radar (C-PAR) located at Beijing Daxing International Airport can provide Z and V<sub>r</sub> observations at a 75-m range resolution over 30 elevation angles ( $0.25^\circ$ – $14.75^\circ$ ) every 2 min. With its high spatiotemporal resolution and high sensitivity to weak echo, C-PAR successfully captured a CI process caused by the collision of two boundary layer convergence lines originated from the thunderstorm outflow in Daxing District of Beijing on 18 June 2020 (X. Zhang et al., 2022). Figure 1 shows that the two boundary layer convergence lines in red rectangle kept approaching each other from 06:30 UTC to 06:42 UTC, and then collided and produced a precipitation echo exceeding 20 dBZ at 06:42 UTC. Yang et al. (2018) used 20 dBZ as the threshold to identify precipitation echoes. Here, we also consider composite Z first exceeding 20 dBZ as the criterion for convection formation (CF). The echo continued to grow and first exceeded 35 dBZ at 06:50 UTC, which met the criterion of CI (Figure 1).

### 2.2. Numerical Model and Data Assimilation Methods

The WRF Model version 4.2.1 was employed in this study. Two one-way nested domains were used. The outer domain d01 had  $404 \times 404$  horizontal grid points with 3-km horizontal grid spacing. The inner domain d02 had  $403 \times 403$  horizontal grid points with 1-km horizontal grid spacing, which covered most of the observation region of C-PAR (Figure 2). Both domains had 51 vertical levels from surface to 10 hPa. The 6-hourly and  $1^\circ \times 1^\circ$  final analyses of the Global Forecast System from the National Centers for Environmental Prediction (FNL/NCEP) was used for constructing initial and boundary conditions. For both model domains, the following model physics schemes were used: the Thompson microphysics scheme (Thompson et al., 2008), the Rapid Radiative Transfer Model for global model longwave radiation scheme (Mlawer et al., 1997), Dudhia shortwave radiation scheme (Dudhia, 1989), revised MM5 surface layer scheme (Jimenez et al., 2012), unified Noah land-surface model scheme (Ek et al., 2003), and Yonsei State University boundary-layer scheme (Hong et al., 2006). Neither d01 nor d02 used any cumulus parameterization scheme.

In this study, C-PAR data were first quality controlled using a radar perusing and editing software called SOLOII developed by National Center for Atmospheric Research (Smith et al., 1995). Some clutter was found in low-level Z data, so Z values below 1 km that were  $<10$  dBZ were removed to minimize the influence from the clutter. Reflectivity values smaller than  $-10$  dBZ above 1 km were also removed following Teng et al. (2020) to ensure data quality. Previous studies have shown that assimilating clear-air Z observations can suppress spurious

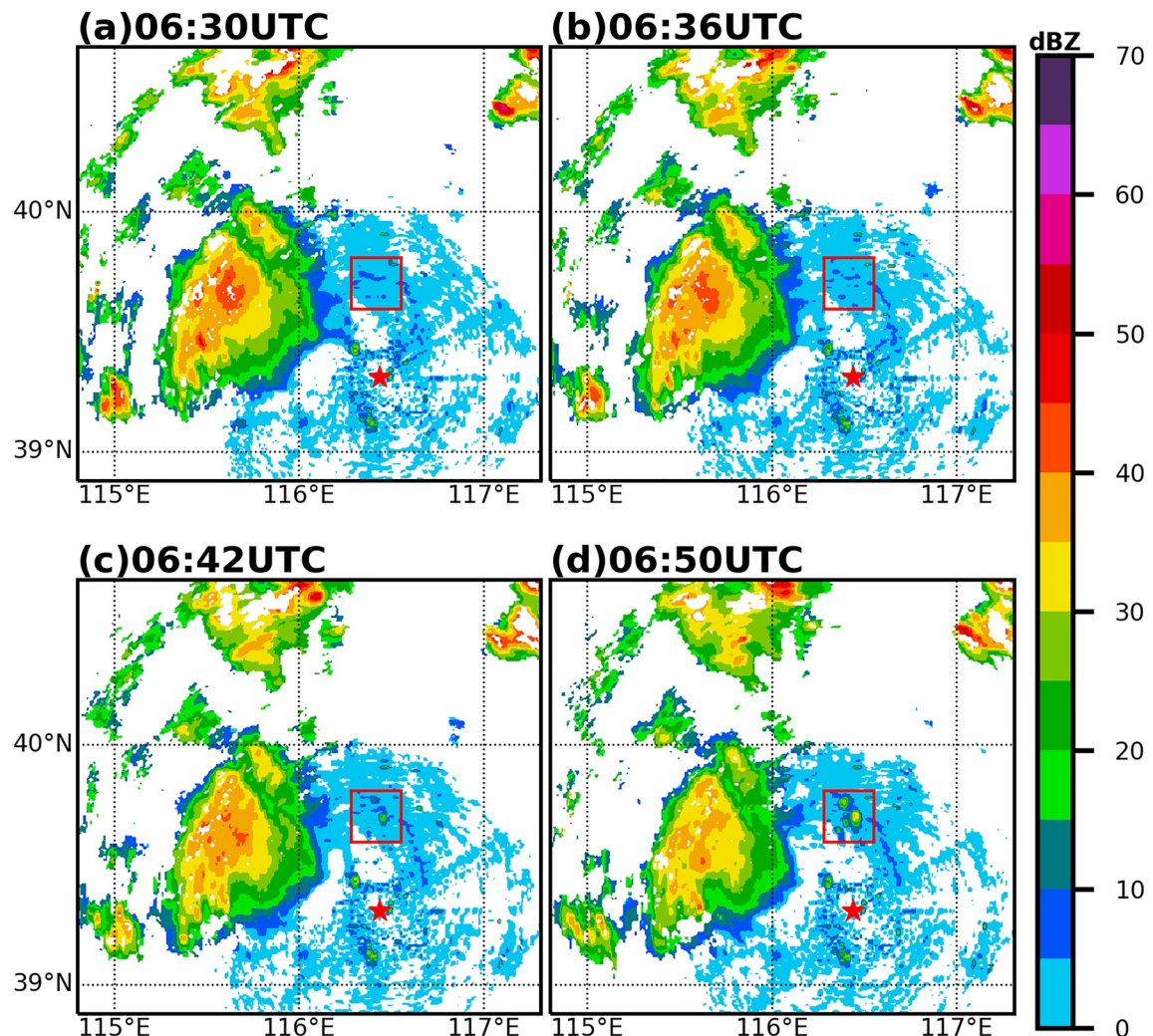


**Figure 1.** (a–d) The composite radar  $Z$  of C-band phased-array radar (C-PAR) at (a) 06:30 UTC, (b) 06:36 UTC, (c) 06:42 UTC, (d) 06:50 UTC, 18 June 2020. The red rectangle highlights the focused convective initiation (CI) area.

convective cells (Aksoy et al., 2009; Huang et al., 2020; Yussouf & Stensrud, 2010). We follow the method to suppress spurious convective cells by randomly selecting 10% of the removed values and set the  $Z$  values to  $-35$  dBZ (default clear-air  $Z$  value in WRF) to ensure comparable amount of  $Z$  data in clear-air region and precipitation region.

We used the same WRF-EnKF system as Wang et al. (2021). The ensemble size was 45. The initial ensemble members were generated using WRF-3DVAR “cv3” options to add random perturbations to the FNL/NCEP analysis at 00:00 UTC 18 June 2020. The perturbed variables included mixing ratio for water vapor, potential temperature, and horizontal wind components. The standard deviations of perturbations were 0.5 g/kg for mixing ratio, 1 K for temperature, and 2 m/s for horizontal winds, respectively (Meng & Zhang, 2007; Zhu et al., 2016). The covariance relaxation method (F. Q. Zhang et al., 2004) was used with a relaxation coefficient of 0.5 for inflating the background error. This study used the successive covariance localization method (F. Zhang et al., 2009). The horizontal localization radius of influence (ROI) was 3 km for both  $V_r$  and  $Z$ . The vertical ROI was set to five vertical model grids for  $Z$  and 15 vertical model grids for  $V_r$ . Due to limitation in computational cost and the spatial resolution of C-PAR, the data thinning was set to 100, which means 1/100 of the total observations were randomly chosen and assimilated, corresponding to  $\sim 1$ -km spatial resolution for C-PAR radar data.

When assimilating reflectivity and radial velocity, the prognostic variables of potential temperature ( $T$ ), perturbation geopotential (PH), temperature at 2 m ( $T_2$ ), surface skin temperature (TSK), perturbation dry air mass in

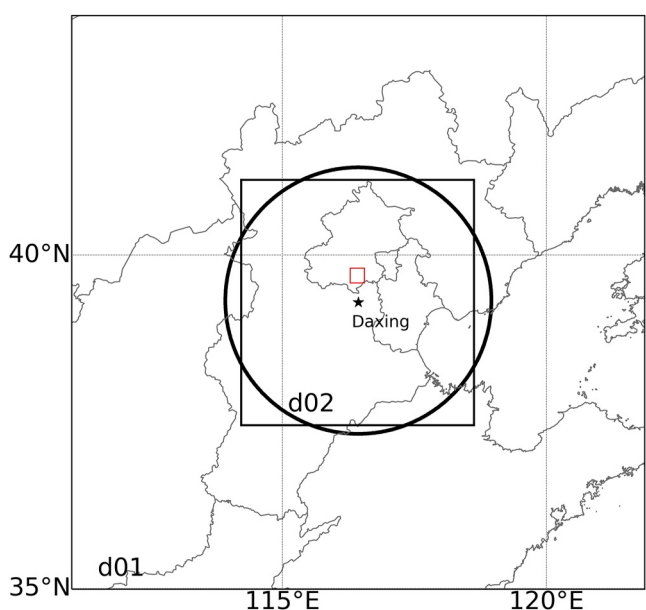


**Figure 2.** The Weather Research and Forecasting simulation domains. The red rectangle highlights the focused convective initiation (CI) area. The location of C-band phased-array radar (C-PAR) is marked with the black star. The black solid circle indicates the C-PAR observation range with radius of 216 km.

column (MU), perturbation pressure ( $P$ ), and surface pressure (PSFC) were updated. To reduce false correlation (Dowell et al., 2011), only when assimilating  $Z$ , the following hydrometeor variables were updated: cloud water mixing ratio (QCLOUD), water mixing ratio (QRRAIN), water vapor mixing ratio (QVAPOR), graupel mixing ratio (QGRAUP), rain cloud ice mixing ratio (QICE), snow mixing ratio (QSNOW), and rain number concentration (NRRAIN). Similarly, only when assimilating  $V_r$ , the following wind variables were updated: horizontal wind components ( $U$  and  $V$ ), vertical velocity ( $W$ ), and 10-m horizontal wind ( $U10$  and  $V10$ ). The observation error for  $V_r$  and  $Z$  was set to 1 m/s and 2 dBZ, respectively.

### 2.3. Experimental Design

Figure 3 shows the flowchart of experiments. First, ensemble forecasts were performed from 00:00 UTC 18 June to 06:00 UTC 18 June to develop a high-resolution, flow-dependent background error covariance. Data assimilation was only performed in d02 from 06:00 UTC to 06:30 UTC with different combinations of assimilation frequency and observation types in different experiments (explained later).

Five experiments were conducted to examine the impact of assimilating different types of C-PAR data. The first experiment (Control) did not assimilate any data. The second experiment (Only\_ref) only assimilated  $Z$  data from C-PAR to examine the impact of changing only the thermodynamic field on CI forecasts. The third experiment (Halfvel\_ref) not only assimilated  $Z$  data but also  $V_r$  data in precipitation region, which aims to examine the impact of

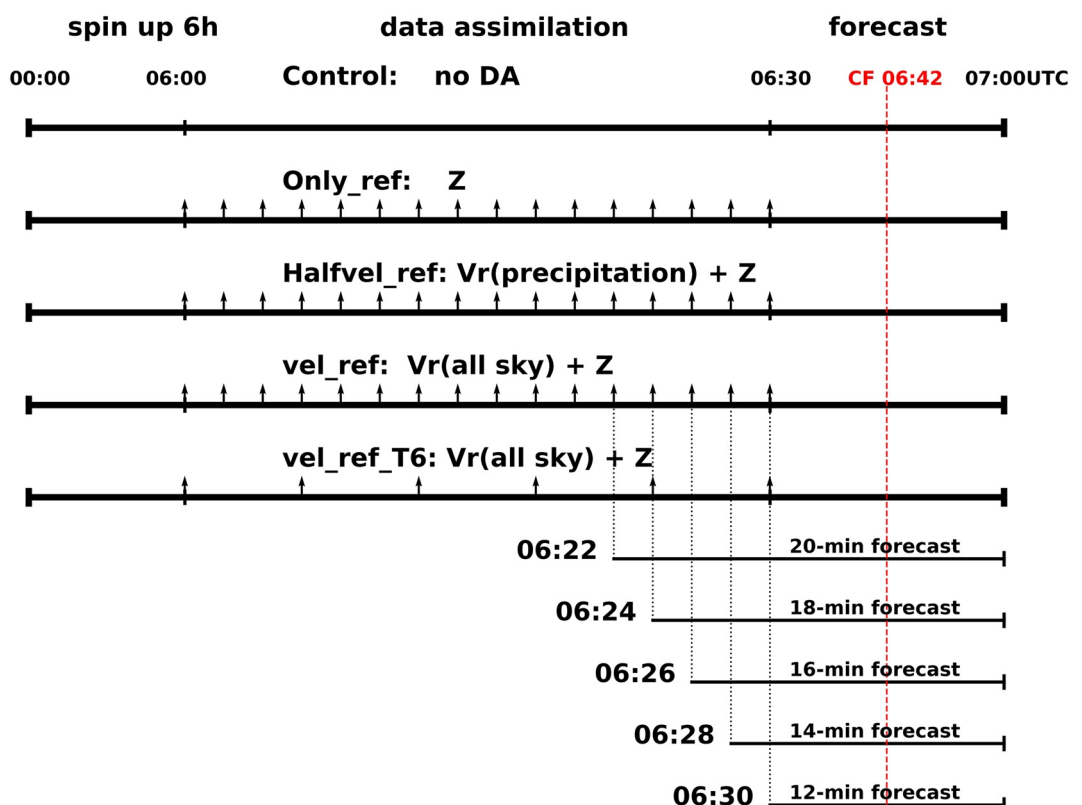


**Figure 3.** Data assimilation and forecast timelines and configurations of the five experiments where the upward pointing arrows indicate the times when radar data were assimilated.

changing dynamic field on CI forecast. The fourth experiment, Vel\_ref, was the same as Halfvel\_ref except that Vr data in the clear-sky region was also assimilated in order to examine its impact on the CI forecast. All of the four aforementioned experiments had an assimilation frequency of every 2 min. To verify the advantage of the high observation frequency of C-PAR in CI forecasting, an additional experiment, Vel\_ref\_T6, was performed, which assimilated same data as the fourth experiment (Vel\_ref) but at a frequency of every 6 min from 06:00 UTC to 06:30 UTC, which the observation frequency similar with traditional doppler radars. After the assimilation, 30-min deterministic forecasts started from 06:30 UTC to 07:00 UTC in the five experiments as mentioned above.

To explore the maximum lead time of CI prediction in this case, five additional deterministic forecasts from experiment Vel\_ref were performed starting from different analysis time at 06:22, 06:24, 06:26, 06:28, and 06:30 UTC.

### 3. Results

#### 3.1. Analysis Results

The root-mean-square innovation (RMSI) were used to objectively quantify the impact of assimilating different types of observation data during the entire assimilation period. As is previously described, the convection was triggered by the collision of two boundary convergence lines. Therefore, in order to examine assimilation effect on low level, RMSI of 0.75° tilt of C-PAR was calculated. Besides, considering calculating RMSI of different sweep angles can be more reliable, referring to Wang et al. (2021) which calculated RMSI of 2.4° tilt of radar, this study also calculated RMSI of 2.25° tilt of C-PAR. Figures 4a and 4c show the RMSI of Z from the first four experiments calculated at the 0.75° tilt and 2.25° tilt, respectively, while Figures 4b and 4d show the RMSI of Vr from the first four experiments calculated at the 0.75° tilt and 2.25° tilt, respectively. Comparing the Control experiment and the other three experiments, the results show that assimilating Z data of C-PAR significantly reduced RMSI of Z (Figures 4a and 4c). However, only assimilating Z data (Only\_ref) increased the RMSI of Vr (compared with Control). Assimilating Vr in precipitating region helped to reduce RMSI of Vr (Halfvel\_ref), and the assimilation of additional clear-sky Vr can further reduce RMSI of Vr (Vel\_ref), which was more obvious in the lower level (Figures 4b and 4d). As such, experiment Vel\_ref had the best overall assimilation performance.

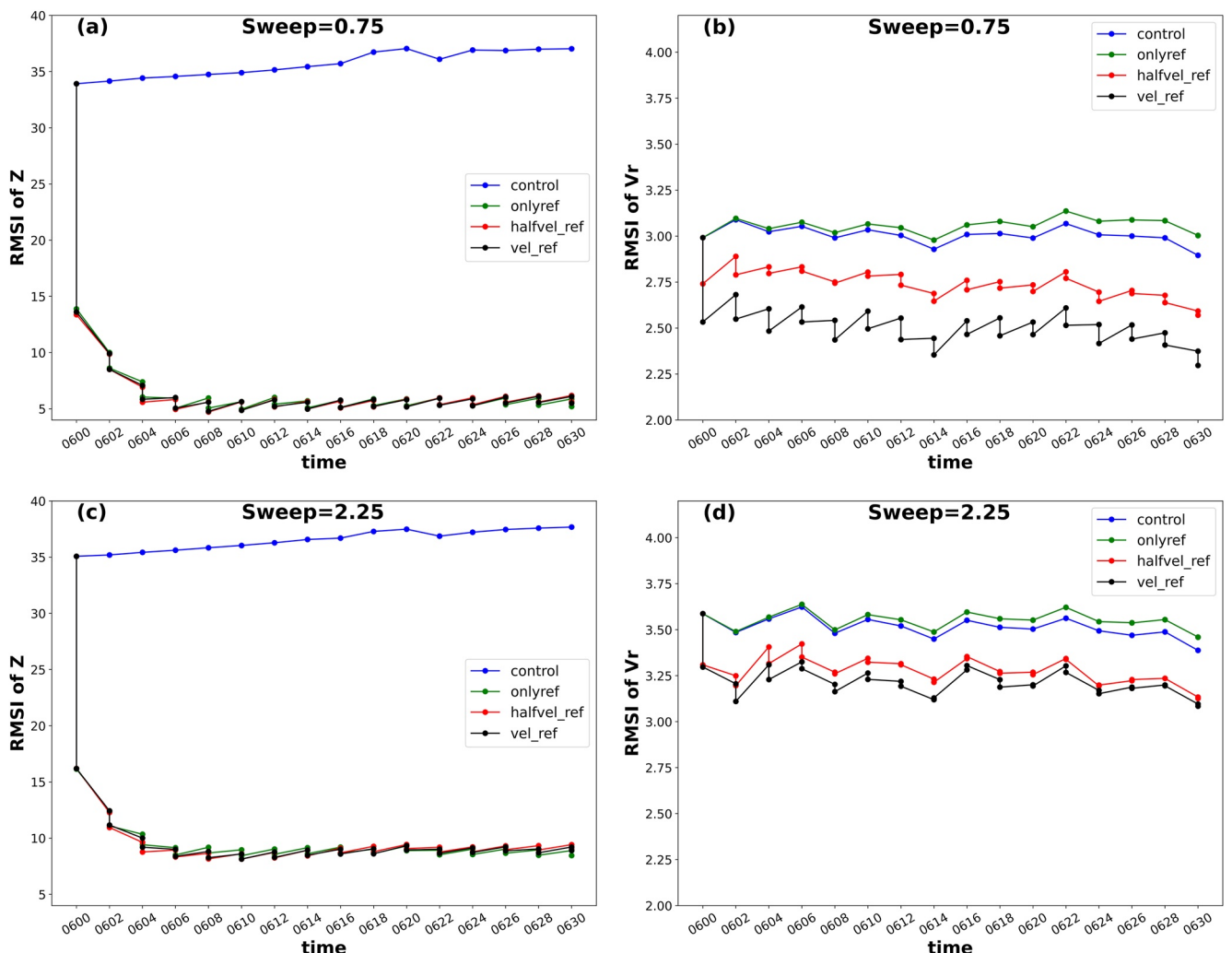
Figure 5 shows the sounding in the focused convection initiation area at 06:30 UTC of the first four experiments. The results show that the basic background environment among Only\_ref, Halfvel\_ref, and Vel\_ref is similar, which indicates that the change in small-scale dynamic field brought by the data assimilation can be important.

Figure 6 shows the EnKF analyses of divergence (multiplied by 103) of horizontal wind and horizontal wind field at 06:30 UTC. After assimilating Vr, the dynamic field changed significantly. At 100 m AGL, considering the location where the CI happened, the location of the center of the wind convergence is more reasonable in Halfvel\_ref experiment and Vel\_ref experiment compared to Only\_ref experiment. Comparing Figures 6c and 6d, after assimilating clear-air Vr, the horizontal wind to the east of the focused convection initiation area changes from south wind to east wind, which shows the influence of assimilating clear-air Vr on the low-level dynamic field and agrees with the low-level Vr observation at the lowest 0.25 tilt (not shown). These results show that assimilating clear-air Vr can improve the low-level wind field, which is important for CI.

#### 3.2. Forecasting Results

The observation results shows that two convection cells were initiated in the concerned region from 06:42 UTC. Convection-A first formed (i.e., with noticeable precipitation) at 06:42 UTC and initiated (i.e., CI) at 06:50 UTC. Convection-B first formed at 06:48 UTC and initiated at 06:54 UTC. Convection-B located to the northwest of Convection-A (Figures 7a1–7a7).

Control experiment shows spurious echoes over 20 dBZ distributed in all over the concerned area and they kept growing over time (Figures 7b1–7b8). Previous studies have demonstrated that adding initial perturbations to the entire computational domain would introduce spurious cells in individual members (Snyder & Zhang, 2003; Tong & Xue, 2005). Such spurious cells can be suppressed by assimilating radar reflectivity in clear-air region. Thus, the spurious echoes produced in the Control experiment are likely to be caused by initial perturbations added to the ensemble members during ensemble initialization and the lack of assimilation of clear-air radar reflectivity to suppress them. Spurious echoes were largely suppressed in Only\_ref initially. However, some



**Figure 4.** (a) The root-mean-square innovation (RMSI) of model Z against 0.75° tilt of C-band phased-array radar (C-PAR) observation before and after each analysis from Control experiment (blue), Only\_ref (green), Halfvel\_ref (red), Vel\_ref (black). (b) is similar as (a) but for RMSI of Vr. (c) and (d) are the same as (a) and (b), but for RMSI calculated at the 2.25° tilt of C-PAR observation.

small spurious convections began to grow since 06:44 UTC (Figures 7c1–7c8). In our EnKF configuration, the wind field ( $U$ ,  $V$ ,  $W$ ,  $U10$ , and  $V10$ ) were only updated when assimilating  $V_r$ . As a result, in Only\_ref experiment, even though the reflectivity data were assimilated and hydrometers in the spurious cells were removed after assimilation, the added perturbations to the dynamic fields were not removed, which can cause spurious cells to grow again in the deterministic forecast. The Control experiment and Only\_ref both failed to forecast CF and CI.

Wang and Xue (2012) assessed CI in three aspects: time, location, and shape. Halfvel\_ref roughly predicted CF and CI. Convection-A and Convection-B were both formed at 06:44 UTC. Compared with observations, Convection-A formed 2 min later and Convection-B formed 4 min earlier. The location of Convection-A and Convection-B was similar with observation. Then, Convection-A initialized at 06:54 UTC while Convection-B initialized at 06:46 UTC in Halfvel\_ref. Convection-A was organized and stronger than Convection-B in observation. However, Halfvel\_ref showed Convection-A was less organized and became a multicell storm, while Convection-B was much stronger and larger than Convection-A (Figures 7d1–7d8). The timing error and the shape error were both obvious in Halfvel\_ref. The wind speed was enhanced than experiments mentioned above, but the convergence of wind was not obvious.

Vel\_ref successfully forecasted both the CF and CI of two convective cells. Convection-A formed at 06:40 UTC while Convection-B formed at 06:50 UTC. Compared with observations, Convection-A formed 2 min earlier in the forecast and Convection-B 2 min later. Convection-A was located ~10 km away from the southwest of

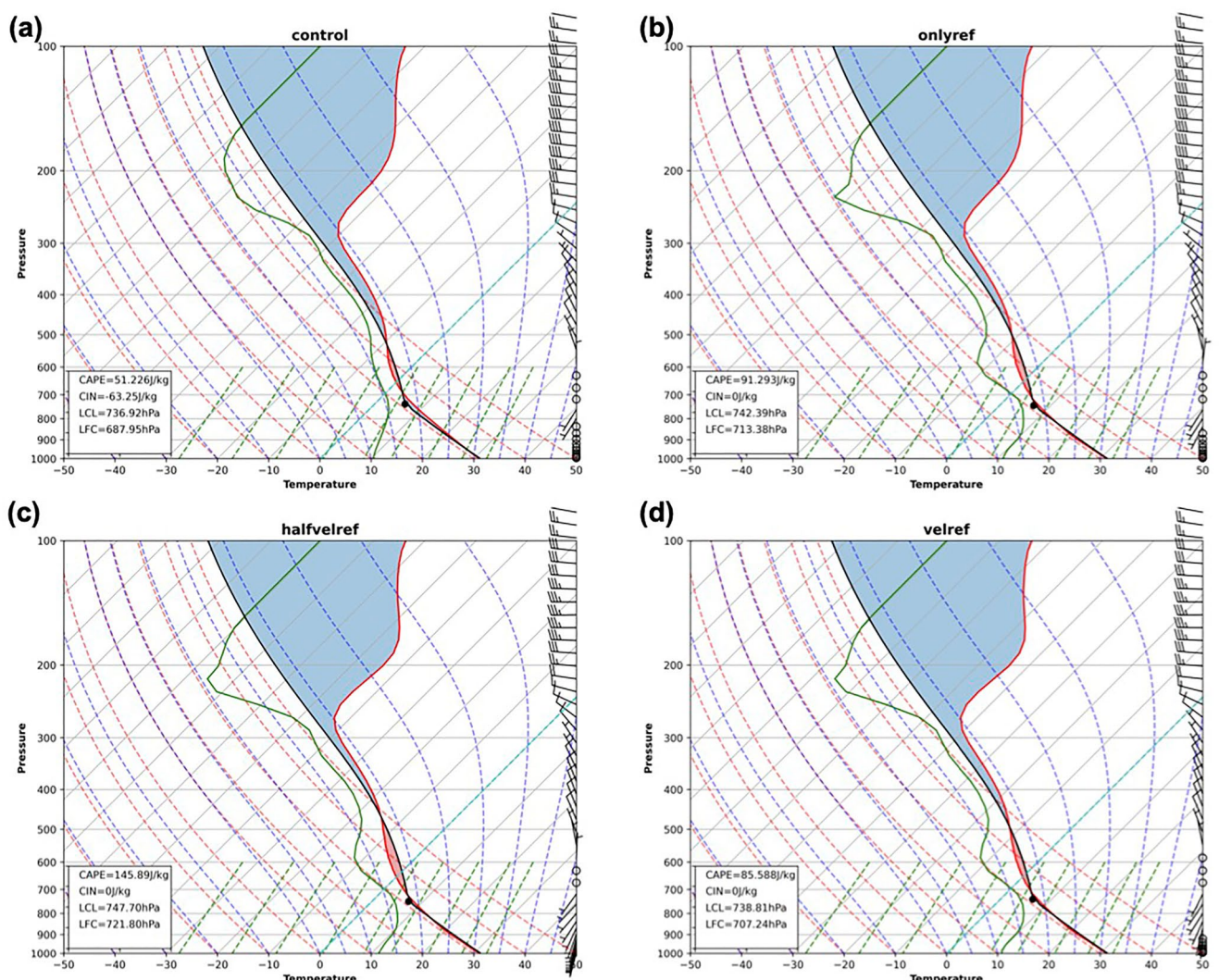


**Figure 5.** Average Skew-T plots of sounding extracted from model forecasts at 06:30 UTC for focused convection initiation area highlighted by the red rectangle in Figure 2 for (a) Control, (b) Only\_ref, (c) Halfvel\_ref, and (d) Vel\_ref experiments.

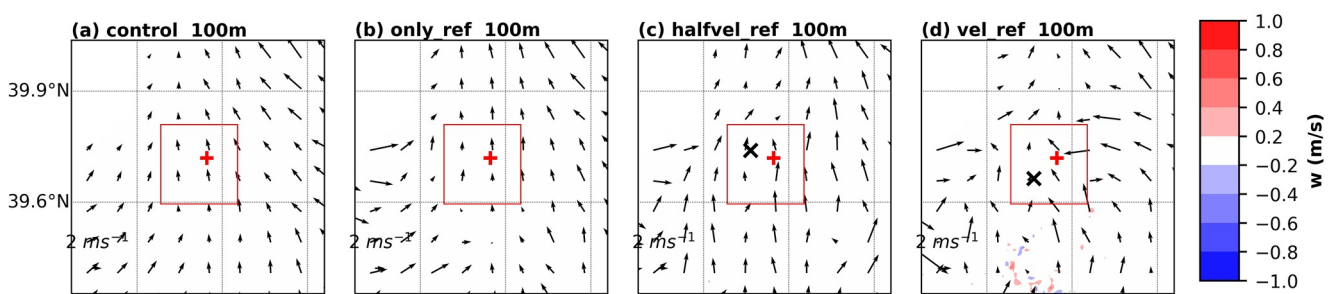


**Figure 6.** The analyzed three-dimensional wind field at the height of 100 m AGL at 06:30 UTC, 18 June 2020 from (a) Control experiment, (b) Only\_ref, (c) Halfvel\_ref, (d) Vel\_ref. The vertical velocity is shown by shade ( $\text{m s}^{-1}$ ), and the horizontal wind field is shown by vector. Red plus sign shows the observation position of convection at 06:42 UTC. Black cross sign shows the position of convection in forecasting results at 06:42 UTC.

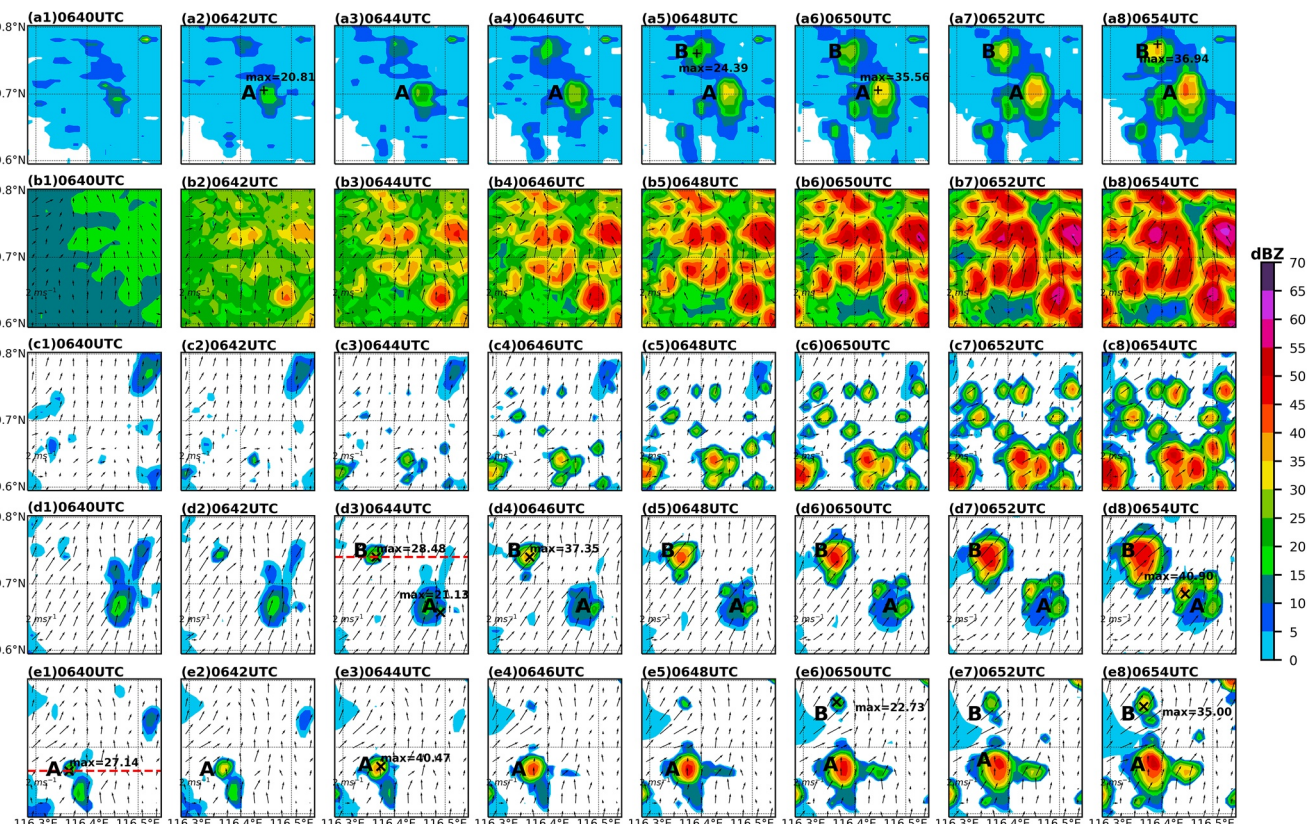


**Figure 7.** Composite Z from radar observation (a1–a8) and forecasted composite Z and 500 m wind started from 06:30 UTC from Control experiment (b1–b8), Only\_ref (c1–c8), Halfvel\_ref (d1–d8), Vel\_ref (e1–e8) shown every 2 min from 06:40 UTC to 06:54 UTC.

radar observation. Convection-B was found to the north of Convection-A, which was similar to observation. Convection-A initialized at 06:44 UTC while Convection-B initialized at 06:54 UTC. Convection-A was 6 min earlier than observation while Convection-B was found at the same time as observation. The shape errors of two convective cells were small in Vel\_ref (Figures 7e1–7e8). Previous studies showed that cloud microphysics, boundary layer processes, and turbulence can all contribute to the uncertainty of numerical forecast model with convection-permitting resolution (Feng et al., 2018; Zhou et al., 2022), which might cause the whole development intensify of Convection-A overestimated. The wind speed in Vel\_ref was weaker than in Halfvel\_ref, but the convergence of wind was stronger, especially around Convection-A.

Figure 8 shows the cross-section of stronger convection in Halfvel\_ref (Figures 8a1–8a4) and Vel\_ref (Figures 8b1–8b4). In the two experiments, water vapor converged at low level and diverged at high level, and rising motion could be seen up to 3.7 km at 06:30 UTC, which was consistent with the conclusion in Section 3.1. The vertical motion and convergence and divergence of water vapor were both enhanced over time in two experiments. Assimilating Vr in the precipitation region can change the dynamic field remarkably, and create interaction between the dynamic field and thermodynamic field to provide more accurate pre-CI environment. After assimilating Vr in the clear air, the vertical upward motion was stronger than Halfvel\_ref, which might cause the remarkable convergence of water vapor and earlier appearance of strong water vapor convergence center at the location of CF. As we know, lift plays a decisive role in CI (Abulikemu et al., 2016), that may explain why the best result is Vel\_ref.

Based on the analysis results and forecasting results mentioned above we can conclude that: although we obtain similar conclusions as past studies that assimilating clear-air Z data can help to suppress the spurious convective cells (Aksoy et al., 2009; Tong & Xue, 2005), we find that only updating the thermodynamic field is insufficient for CI in this case. Assimilating Vr in the precipitation region can update dynamic fields dramatically and provide suitable pre-CI environment. However, due to the lack of clear-air information, the dynamic fields in clear-air region were not optimal, which might degrade the forecast accuracy.

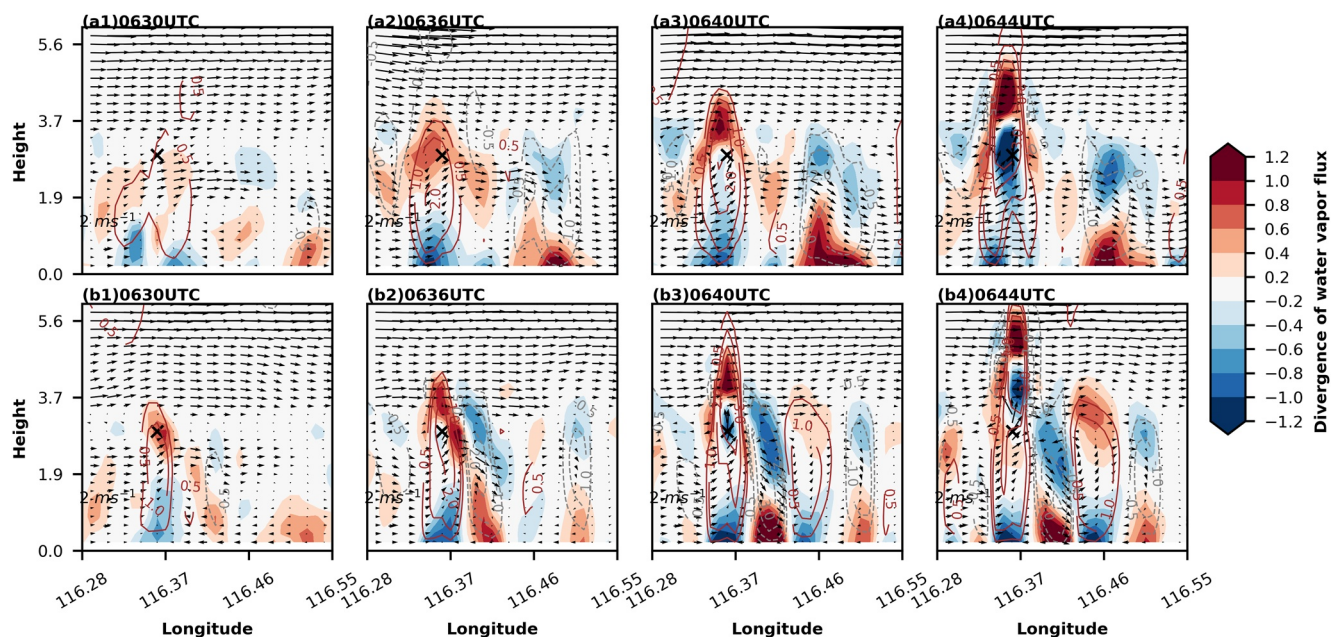


**Figure 8.** Cross-section of vertical velocity (brown solid lines contour at 0.5, 1, 2, and 3  $\text{m s}^{-1}$  and gray dashed lines contour at  $-0.5, -1, -2$ , and  $-3 \text{ m s}^{-1}$ ), wind (vectors,  $\text{m s}^{-1}$ ) and the convergence of water vapor flux and the divergence of water vapor flux at 06:30, 06:36, 06:40 and 06:44 UTC from experiments Halfvel\_ref (a1–a4) and Vel\_ref (b1–b4) along in the lines in Figures 7d3 and 7e1, respectively. The black cross symbol is the location of Z first exceeding 20 dBZ.

The result of Vel\_ref was the best among the four experiments. An additional experiment, Vel\_ref\_T6, was performed based on Vel\_ref that has 6-min data assimilation interval to explore the necessity of high data assimilation frequency provided by C-PAR. Compared with Vel\_ref (Figures 9c1–9c3), Vel\_ref\_T6 (Figures 9b1–9b3) not only forecasted more spurious echo than Vel\_ref but also failed to predict the CI process. The result of Vel\_ref is obviously better than Vel\_ref\_T6.

Furthermore, we performed additional deterministic forecasts to explore the maximum lead time of CI prediction in Vel\_ref. First, we discussed the forecast results initialized from 06:22 UTC (Figures 10b1–10b7), 06:24 UTC (Figures 10c1–10c7), and 06:26 UTC (Figures 10d1–10d7). They all failed to forecast Convection-B. As for Convection-A, they all successfully forecasted it, although they overestimated its strength. Convection-A was all located  $\sim 10$  km southwest from observation, its formation timing error was all  $< 5$  min, and the time of its CI was all at 06:44 UTC.

The forecasts started from 06:28 UTC (Figures 10e1–10e7) and 06:30 UTC (Figures 10f1–10f7) both successfully captured formation and initiation of Convection-A and Convection-B. The timing error of two CF events was both  $< 5$  min. The timing error of Convection-A initiation was both  $> 5$  min but  $< 10$  min, while the timing error of Convection-B initiation  $< 5$  min. Convection-A was both located  $\sim 10$  km southwest from observation, while the Convection-B was both located similar to observation. Some spurious convection cells were formed near Convection-A, but the size and strength of those convection cells were smaller and weaker in the forecast starting from 06:30 UTC.

#### 4. Summary and Discussion

On 18 June 2020, C-PAR captured a complete CI process caused by the collision of two boundary layer convergence lines in the clear sky region. This study used WRF-EnKF with 45 ensemble members to assimilate C-PAR Z and Vr data to investigate the impact of assimilating PAR data on the forecast of a real CI case. Each ensemble members had two one-way nested WRF model domains with 3-km grid spacing for the outer domain and 1-km grid spacing for the inner domain. After 6 hr spin up, the radar observations were only assimilated in the inner domain starting from 06:00 UTC.

We designed four experiments to explore the impact of assimilating Z or Vr from C-PAR on the forecasts of CF and CI. Assimilating clear-sky Vr is conducive for accurate simulation of dynamic field by enhancing vertical motion, correcting the location of wind convergence and divergence and then influence the thermodynamic field. The interaction of dynamic field and thermodynamic field provides great pre-CI environment, which plays a key

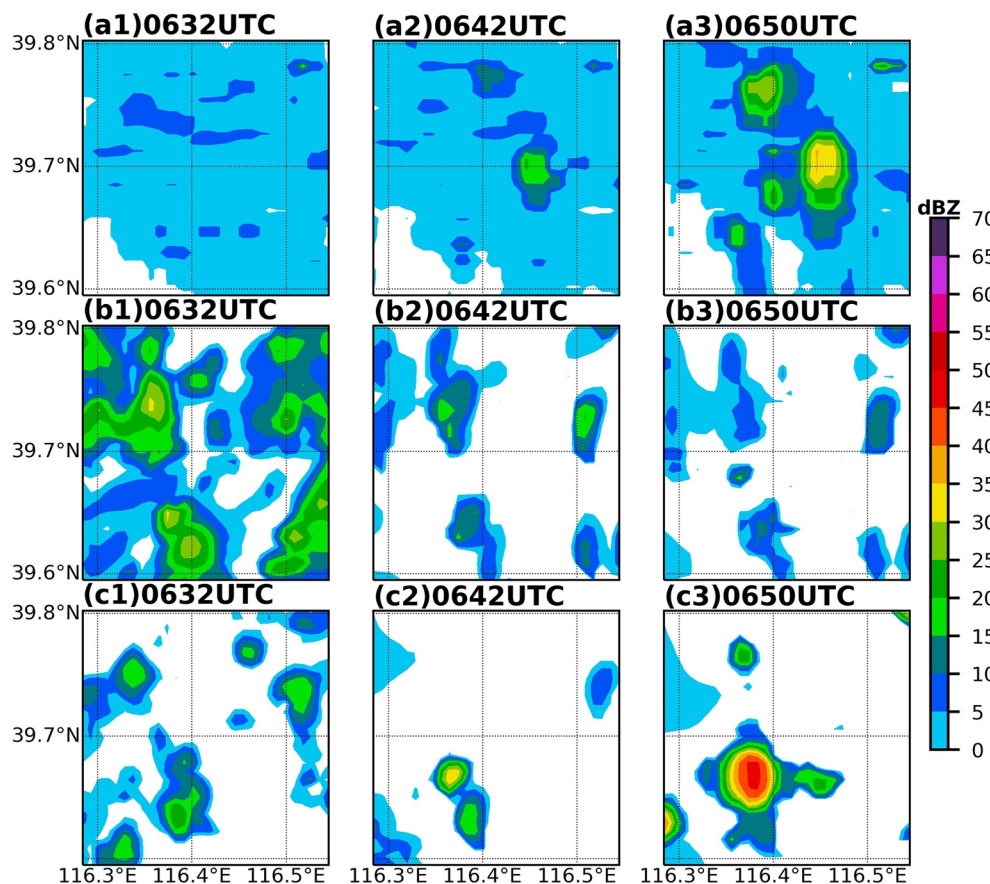


**Figure 9.** The composite reflectivity of (a1–a3) radar observation, (b1–b3) Vel\_ref\_T6, (c1–c3) Vel\_ref at 06:32, 06:42, and 06:50 UTC. The red rectangle highlights the focused convection initiation area.

role on CI forecasts. Assimilating clear-sky Vr has an obvious advantage in improving the forecast accuracy of CI and is conducive for forecasting correct shape of convection. Our results have verified Huang et al. (2022), which proposed that assimilating clear-air Vr can offer potential benefits, from a real-case study aspect.

Previous study proved the benefits of high-frequency assimilation of PAR data for small-scale severe weather process (Stratman et al., 2020; Wang et al., 2021). We also explore the impact of high-frequency assimilating PAR data on CI forecast. The result shows high-frequency assimilation of PAR data not only helps to suppress spurious echoes but also conducive for accurate CI forecasts in this case study that is similar with previous study.

Furthermore, as Stensrud et al. (2009) believes that the eventual goal of storm-scale radar DA and forecasts is to extend lead times of severe weather warning. Based on the best forecast results (Vel\_ref), we have explored the maximum lead time of CI by conducting deterministic forecasts from different data assimilation cycles to analyze the impact on the timing of CI after assimilating clear-sky Vr. The maximum lead time of data assimilation in this case is 20 min. Although displacement errors of convection could be found in all forecasts, prediction of convection shape would be better if forecast was initialized within 15 min in advance.

In conclusion, this study is the first real-case study to investigate the benefits of assimilating high spatiotemporal resolution PAR clear-air Vr data for the CI process. We suggest that PAR opens up promising prospect for nowcasting of severe convective weather, not only for filling the gaps in current operational observing systems but also for numerical prediction of rapid developing mesoscale processes. However, as Huang et al. (2022) mentioned, various reasons (different combination of CI mechanisms, heterogeneous atmospheric environment, uncertainties different scales, etc.) influence the CI forecasts. Therefore, more cases are needed to further verify the potential improvements in the future. Besides, previous studies have demonstrated the benefits of assimilating PAR data with finer grid spacing resolution (Maejima et al., 2017; Miyoshi et al., 2016; Wang et al., 2021).

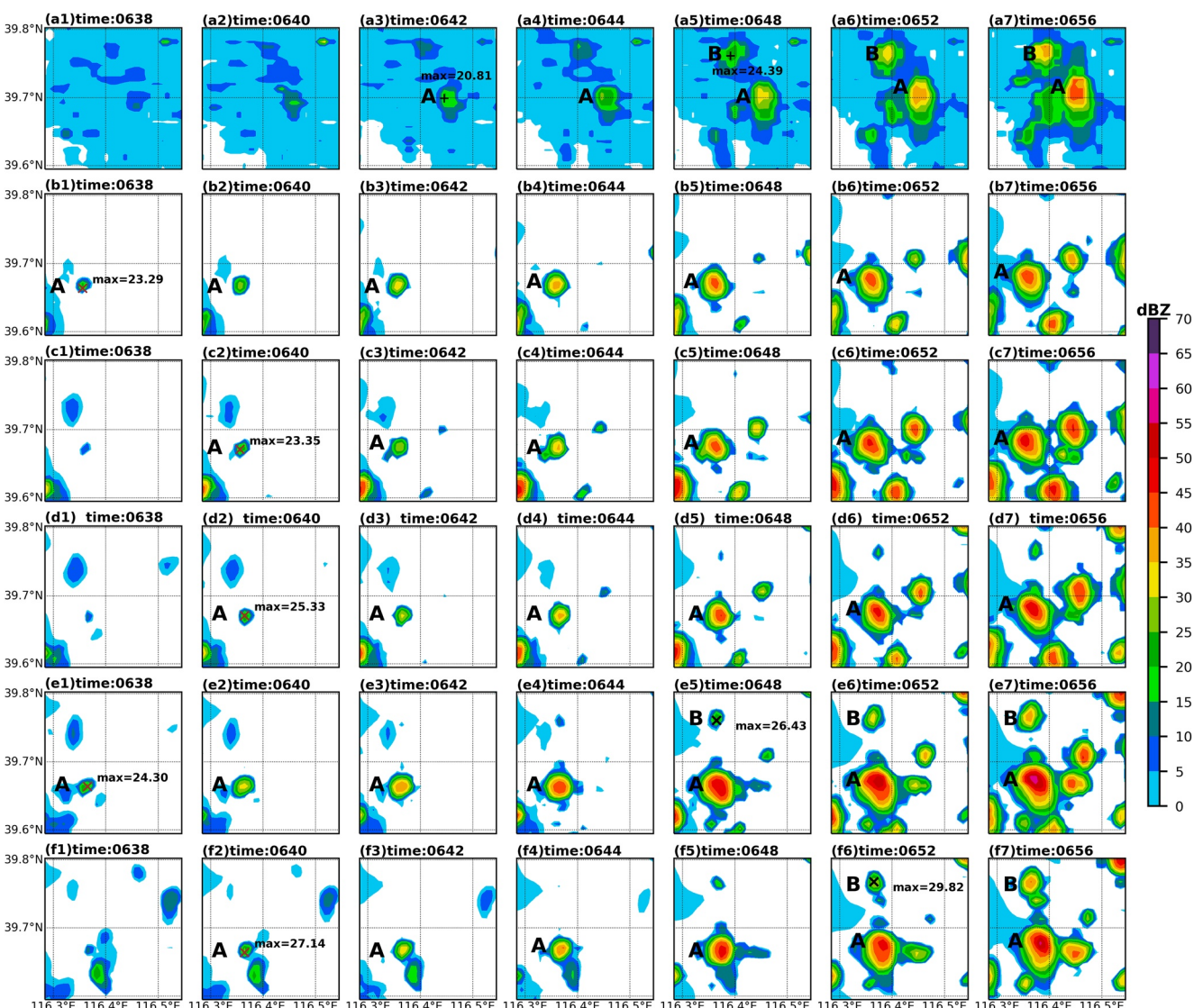


**Figure 10.** Composite Z from radar observation (a1–a7) and forecasts started from 06:22 UTC (b1–b7), 06:24 UTC (c1–c7), 06:26 UTC (d1–d7), 06:28 UTC (e1–e7), and 06:30 UTC (f1–f7) corresponding to 06:38, 06:40, 06:42, 06:44, 06:48, 06:52, and 06:56 UTC.

Limited by computing resource, we chose horizontal grid spacing of 1 km in this case study, which might be a limitation on forecasting results. Moreover, Taylor et al. (2023) suggested that lowering the localization scale parameter might reduce the buildup of convective instability and stronger winds in the analyses which promote the growth of spurious and strong convection, which is worthy to be investigated in future research.

#### Acknowledgments

This work was primarily supported by the National Natural Science Foundation of China (Grants 42230607, 42025501, 41875053, 42192555, 42175159, and 61827901), the National Key Research and Development Program of China (Grant 2017YFC1501703), Fundamental Research Funds for the Central Universities (020714380171 and 020714380177), as well as the Open Grants of the State Key Laboratory of Severe Weather (Grants 2021LASW-A01 and 2022LASW-A01).

#### Data Availability Statement

The observation data used in EnKF are available at Gong (2022).

#### References

- Abulikemu, A., Xu, X., Wang, Y., Ding, J. F., Zhang, S. S., & Shen, W. Q. (2016). A modeling study of convection initiation prior to the merger of a sea-breeze front and a gust front. *Atmospheric Research*, 182, 10–19. <https://doi.org/10.1016/j.atmosres.2016.07.003>
- Aksoy, A., Dowell, D. C., & Snyder, C. (2009). A multicase comparative assessment of the ensemble Kalman filter for assimilation of radar observations. Part I: Storm-scale analyses. *Monthly Weather Review*, 137(6), 1805–1824. <https://doi.org/10.1175/2008mwr2691.1>
- Burghardt, B. J., Evans, C., & Roebber, P. J. (2014). Assessing the predictability of convection initiation in the high plains using an object-based approach. *Weather and Forecasting*, 29(2), 403–418. <https://doi.org/10.1175/waf-d-13-00089.1>

- Chen, M., Xiao, X., & Gao, F. (2017). Dynamical effect of outflow boundary on localized initiation and rapid enhancement of severe convection over Beijing-Tianjin-Hebei region. *Chinese Journal of Atmospheric Sciences*, 41(5), 897–917.
- Childs, P. P., Qureshi, A. L., Raman, S., Alapaty, K., Ellis, R., Boyles, R., & Niyogi, D. (2006). Simulation of convective initiation during IHOP\_2002 using the flux-adjusting surface data assimilation system (FASDAS). *Monthly Weather Review*, 134(1), 134–148. <https://doi.org/10.1175/mwr3064.1>
- Clark, P. A., Browning, K. A., Morcrette, C. J., Blyth, A. M., Forbes, R. M., Brooks, B., & Perry, F. (2014). The evolution of an MCS over southern England. Part 1: Observations. *Quarterly Journal of the Royal Meteorological Society*, 140(679), 439–457. <https://doi.org/10.1002/qj.2138>
- Coniglio, M. C., Romine, G. S., Turner, D. D., & Torn, R. D. (2019). Impacts of targeted AERI and Doppler lidar wind retrievals on short-term forecasts of the initiation and early evolution of thunderstorms. *Monthly Weather Review*, 147(4), 1149–1170. <https://doi.org/10.1175/mwr-d-18-0351.1>
- Degelia, S. K., Wang, X. G., Stensrud, D. J., & Johnson, A. (2018). Understanding the impact of radar and in situ observations on the prediction of a nocturnal convection initiation event on 25 June 2013 using an ensemble-based multiscale data assimilation system. *Monthly Weather Review*, 146(6), 1837–1859. <https://doi.org/10.1175/mwr-d-17-0128.1>
- Dowell, D. C., Wicker, L. J., & Snyder, C. (2011). Ensemble Kalman filter assimilation of radar observations of the 8 May 2003 Oklahoma City supercell: Influences of reflectivity observations on storm-scale analyses. *Monthly Weather Review*, 139(1), 272–294. <https://doi.org/10.1175/2010mwr3438.1>
- Dudhia, J. (1989). Numerical study of convection observed during the winter monsoon experiment using a mesoscale two-dimensional model. *Journal of the Atmospheric Sciences*, 46(20), 3077–3107. [https://doi.org/10.1175/1520-0469\(1989\)046<3077:nsocod>2.0.co;2](https://doi.org/10.1175/1520-0469(1989)046<3077:nsocod>2.0.co;2)
- Ek, M. B., Mitchell, K. E., Lin, Y., Rogers, E., Grunmann, P., Koren, V., et al. (2003). Implementation of Noah land surface model advances in the National Centers for Environmental Prediction operational mesoscale Eta model. *Journal of Geophysical Research*, 108(D22), 8851. <https://doi.org/10.1029/2002JD003296>
- Evensen, G. (1994). Sequential data assimilation with a nonlinear quasi-geostrophic model using Monte-Carlo methods to forecast error statistics. *Journal of Geophysical Research*, 99(C5), 10143–10162. <https://doi.org/10.1029/94JC00572>
- Fabry, F., & Meunier, V. (2020). Why are radar data so difficult to assimilate skillfully? *Monthly Weather Review*, 148(7), 2819–2836. <https://doi.org/10.1175/mwr-d-19-0374.1>
- Feng, Z., Leung, L. R., Houze, R. A., Hagos, S., Hardin, J., Yang, Q., et al. (2018). Structure and evolution of mesoscale convective systems: Sensitivity to cloud microphysics in convection-permitting simulations over the United States. *Journal of Advances in Modeling Earth Systems*, 10, 1470–1494. <https://doi.org/10.1029/2018MS001305>
- Gasperoni, N. A., Wang, X. G., Brewster, K. A., & Carr, F. H. (2018). Assessing impacts of the high-frequency assimilation of surface observations for the forecast of convection initiation on 3 April 2014 within the Dallas-Fort Worth test bed. *Monthly Weather Review*, 146(11), 3845–3872. <https://doi.org/10.1175/mwr-d-18-0177.1>
- Gebauer, J. G., Shapiro, A., Fedorovich, E., & Klein, P. (2018). Convection initiation caused by heterogeneous low-level jets over the great plains. *Monthly Weather Review*, 146(8), 2615–2637. <https://doi.org/10.1175/mwr-d-18-0002.1>
- Gong, P. (2022). Impacts of assimilating C-band phased-array radar data with EnKF on the forecast of convection initiation: A case study in Beijing, China (version 1) [Dataset]. Zenodo. <https://doi.org/10.5281/zenodo.7471092>
- Honda, T., Amemiya, A., Otsuka, S., Lien, G., Taylor, J., Maejima, Y., et al. (2022). Development of the real-time 30-s-update big data assimilation system for convective rainfall prediction with phased array weather radar: Description and preliminary evaluation. *Journal of Advances in Modeling Earth Systems*, 14, e2021MS002823. <https://doi.org/10.1029/2021MS002823>
- Honda, T., Amemiya, A., Otsuka, S., Taylor, J., Maejima, Y., Nishizawa, S., et al. (2022). Advantage of 30-s-updating numerical weather prediction with a phased-array weather radar over operational nowcast for a convective precipitation system. *Geophysical Research Letters*, 49, e2021GL096927. <https://doi.org/10.1029/2021GL096927>
- Hong, S. Y., Noh, Y., & Dudhia, J. (2006). A new vertical diffusion package with an explicit treatment of entrainment processes. *Monthly Weather Review*, 134(9), 2318–2341. <https://doi.org/10.1175/mwr3199.1>
- Houtekamer, P. L., & Mitchell, H. L. (1998). Data assimilation using an ensemble Kalman filter technique. *Monthly Weather Review*, 126(3), 796–811. [https://doi.org/10.1175/1520-0493\(1998\)126<796:dauaek>2.0.co;2](https://doi.org/10.1175/1520-0493(1998)126<796:dauaek>2.0.co;2)
- Huang, Y., Wang, X., Mahre, A., Yu, T.-Y., & Bodine, D. (2022). Impacts of assimilating future clear-air radial velocity observations from phased array radar on convection initiation forecasts: An observing system simulation experiment study. *Monthly Weather Review*, 150(7), 1563–1583. <https://doi.org/10.1175/mwr-d-21-0199.1>
- Huang, Y. J., Wang, X. G., Kerr, C., Mahre, A., Yu, T. Y., & Bodine, D. (2020). Impact of assimilating future clear-air radial velocity observations from phased-array radar on a supercell thunderstorm forecast: An observing system simulation experiment study. *Monthly Weather Review*, 148(9), 3825–3845. <https://doi.org/10.1175/mwr-d-19-0391.1>
- Jimenez, P. A., Dudhia, J., Gonzalez-Rouco, J. F., Navarro, J., Montavez, J. P., & Garcia-Bustamante, E. (2012). A revised scheme for the WRF surface layer formulation. *Monthly Weather Review*, 140(3), 898–918. <https://doi.org/10.1175/mwr-d-11-00056.1>
- Johnson, A., Wang, X. G., Carley, J. R., Wicker, L. J., & Karstens, C. (2015). A comparison of multiscale GSI-based EnKF and 3DVar data assimilation using radar and conventional observations for midlatitude convective-scale precipitation forecasts. *Monthly Weather Review*, 143(8), 3087–3108. <https://doi.org/10.1175/mwr-d-14-00345.1>
- Keclik, A. M., Evans, C., Roeberer, P. J., & Romine, G. S. (2017). The influence of assimilated upstream, preconvective dropsonde observations on ensemble forecasts of convection initiation during the mesoscale predictability experiment. *Monthly Weather Review*, 145(12), 4747–4770. <https://doi.org/10.1175/mwr-d-17-0159.1>
- Lien, G. Y., Miyoshi, T., Nishizawa, S., Yoshida, R., Yashiro, H., Adachi, S. A., et al. (2017). The near-real-time SCALE-LETKF system: A case of the September 2015 Kanto-Tohoku heavy rainfall. *SOLA*, 13, 1–6. <https://doi.org/10.2151/sola.2017-001>
- Lin, X. X., Feng, Y. R., Xu, D. S., Jian, Y. T., Huang, F., & Huang, J. C. (2022). Improving the nowcasting of strong convection by assimilating both wind and reflectivity observations of phased array radar: A case study. *Journal of Meteorological Research*, 36(1), 61–78. <https://doi.org/10.1007/s13351-022-1034-5>
- Lock, N. A., & Houston, A. L. (2014). Empirical examination of the factors regulating thunderstorm initiation. *Monthly Weather Review*, 142(1), 240–258. <https://doi.org/10.1175/mwr-d-13-00082.1>
- Madaus, L. E., & Hakim, G. J. (2017). Constraining ensemble forecasts of discrete convective initiation with surface observations. *Monthly Weather Review*, 145(7), 2597–2610. <https://doi.org/10.1175/mwr-d-16-0395.1>
- Maejima, Y., Kunii, M., & Miyoshi, T. (2017). 30-second-update 100-m-Mesh data assimilation experiments: A sudden local rain case in Kobe on 11 September 2014. *SOLA*, 13, 174–180. <https://doi.org/10.2151/sola.2017-032>
- Markowski, P., Hannon, C., & Rasmussen, E. (2006). Observations of convection initiation “failure” from the 12 June 2002 IHOP deployment. *Monthly Weather Review*, 134(1), 375–405. <https://doi.org/10.1175/mwr3059.1>

- Meng, Z. Y., & Zhang, F. Q. (2007). Tests of an ensemble kalman filter for mesoscale and regional-scale data assimilation. Part II: Imperfect model experiments. *Monthly Weather Review*, 135(4), 1403–1423.
- Meng, Z. Y., & Zhang, F. Q. (2008a). Tests of an ensemble Kalman filter for mesoscale and regional-scale data assimilation. Part III: Comparison with 3DVAR in a real-data case study. *Monthly Weather Review*, 136(2), 522–540. <https://doi.org/10.1175/2007mwr2106.1>
- Meng, Z. Y., & Zhang, F. Q. (2008b). Tests of an ensemble Kalman filter for mesoscale and regional-scale data assimilation. Part IV: Comparison with 3DVAR in a month-long experiment. *Monthly Weather Review*, 136(10), 3671–3682. <https://doi.org/10.1175/2008mwr2270.1>
- Meng, Z. Y., & Zhang, F. Q. (2011). Limited-area ensemble-based data assimilation. *Monthly Weather Review*, 139(7), 2025–2045. <https://doi.org/10.1175/2011mwr3418.1>
- Miyoshi, T., Kunii, M., Ruiz, J., Lien, G. Y., Satoh, S., Ushio, T., et al. (2016). “Big data assimilation” revolutionizing severe weather prediction. *Bulletin of the American Meteorological Society*, 97(8), 1347–1354. <https://doi.org/10.1175/bams-d-15-00144.1>
- Mlawer, E. J., Taubman, S. J., Brown, P. D., Iacono, M. J., & Clough, S. A. (1997). Radiative transfer for inhomogeneous atmospheres: RRTM, a validated correlated-k model for the longwave. *Journal of Geophysical Research*, 102(D14), 16663–16682. <https://doi.org/10.1029/97JD00237>
- Rennie, S. J., Dance, S. L., Illingworth, A. J., Ballard, S. P., & Simonin, D. (2011). 3D-Var assimilation of insect-derived doppler radar radial winds in convective cases using a high-resolution model. *Monthly Weather Review*, 139(4), 1148–1163. <https://doi.org/10.1175/2010mwr3482.1>
- Smith, S. D., Oye, R., Lee, W. C., & Amer Meteorol, S. O. C. (1995). Solo: Window based software for perusing and editing radar data. In *Paper presented at 9th Symposium on Meteorological Observations and Instrumentation, Charlotte, NC, March 27–31*.
- Snook, N., Xue, M., & Jung, Y. S. (2011). Analysis of a Tornadic mesoscale convective vortex based on ensemble Kalman filter assimilation of CASA X-band and WSR-88D radar data. *Monthly Weather Review*, 139(11), 3446–3468. <https://doi.org/10.1175/mwr-d-10-05053.1>
- Snyder, C., & Zhang, F. Q. (2003). Assimilation of simulated Doppler radar observations with an ensemble Kalman filter. *Monthly Weather Review*, 131(8), 1663–1677. <https://doi.org/10.1175/2555.1>
- Sobash, R. A., & Stensrud, D. J. (2015). Assimilating surface mesonet observations with the EnKF to improve ensemble forecasts of convection initiation on 29 May 2012. *Monthly Weather Review*, 143(9), 3700–3725. <https://doi.org/10.1175/mwr-d-14-00126.1>
- Stensrud, D. J., Xue, M., Wicker, L. J., Kelleher, K. E., Foster, M. P., Schaefer, J. T., et al. (2009). Convective-scale warn-on-forecast system. *Bulletin of the American Meteorological Society*, 90(10), 1487–1499.
- Stratman, D. R., Yussouf, N., Jung, Y. S., Supinie, T. A., Xue, M., Skinner, P. S., & Putnam, B. J. (2020). Optimal temporal frequency of NSSL phased array radar observations for an experimental warn-on-forecast system. *Weather and Forecasting*, 35(1), 193–214. <https://doi.org/10.1175/waf-d-19-0165.1>
- Sun, J. Z., Xue, M., Wilson, J. W., Zawadzki, I., Ballard, S. P., Onylee-Hooimeyer, J., et al. (2014). Use of NWP for nowcasting convective precipitation. *Bulletin of the American Meteorological Society*, 95(3), 409–426. <https://doi.org/10.1175/bams-d-11-00263.1>
- Supinie, T. A., Yussouf, N., Jung, Y. S., Xue, M., Cheng, J., & Wang, S. Z. (2017). Comparison of the analyses and forecasts of a Tornadic supercell storm from assimilating phased-array radar and WSR-88D observations. *Weather and Forecasting*, 32(4), 1379–1401. <https://doi.org/10.1175/waf-d-16-0159.1>
- Taylor, J., Honda, T., Amemiya, A., Otsuka, S., Maejima, Y., & Miyoshi, T. (2023). Sensitivity to localization radii for an ensemble filter numerical weather prediction system with 30-second update. *Weather and Forecasting*, 38(4), 611–632. <https://doi.org/10.1175/waf-d-21-0177.1>
- Teng, Y., Chen, H., Ma, S., Li, S., Wu, D., & Zhou, Y. (2020). The cause of night clear air echo of S-band weather radar in Beijing. *Journal of Applied Meteorological Science*, 31(5), 595–607.
- Thompson, G., Field, P. R., Rasmussen, R. M., & Hall, W. D. (2008). Explicit forecasts of winter precipitation using an improved bulk micro-physics scheme. Part II: Implementation of a new snow parameterization. *Monthly Weather Review*, 136(12), 5095–5115. <https://doi.org/10.1175/2008mwr2387.1>
- Tong, M. J., & Xue, M. (2005). Ensemble Kalman filter assimilation of Doppler radar data with a compressible nonhydrostatic model: OSS experiments. *Monthly Weather Review*, 133(7), 1789–1807. <https://doi.org/10.1175/mwr2898.1>
- Wang, C., Chen, M., & Chen, Y. D. (2022). Impact of combined assimilation of wind profiler and Doppler radar data on a convective-scale cycling forecasting system. *Monthly Weather Review*, 150(2), 431–450. <https://doi.org/10.1175/mwr-d-20-0383.1>
- Wang, C., Zhao, K., Zhu, K. F., Huang, H., Lu, Y. H., Yang, Z. W., et al. (2021). Assimilation of X-band phased-array radar data with EnKF for the analysis and warning forecast of a Tornadic storm. *Journal of Advances in Modeling Earth Systems*, 13, e2020MS002441. <https://doi.org/10.1029/2020MS002441>
- Wang, Q. W., & Xue, M. (2012). Convective initiation on 19 June 2002 during IHOP: High-resolution simulations and analysis of the mesoscale structures and convection initiation. *Journal of Geophysical Research*, 117, D12107. <https://doi.org/10.1029/2012JD017552>
- Weckwerth, T. M., Hanesiak, J., Wilson, J. W., Trier, S. B., Degelia, S. K., Gallus, W. A., et al. (2019). Nocturnal convection initiation during PECAN 2015. *Bulletin of the American Meteorological Society*, 100(11), 2223–2239. <https://doi.org/10.1175/bams-d-18-0299.1>
- Weckwerth, T. M., & Parsons, D. B. (2006). A review of convection initiation and motivation for IHOP\_2002. *Monthly Weather Review*, 134(1), 5–22. <https://doi.org/10.1175/mwr3067.1>
- Weckwerth, T. M., Parsons, D. B., Koch, S. E., Moore, J. A., LeMone, M. A., Demoz, B. B., et al. (2004). An overview of the International H<sub>2</sub>O Project (IHOP\_2002) and some preliminary highlights. *Bulletin of the American Meteorological Society*, 85(2), 253–277. <https://doi.org/10.1175/bams-85-2-253>
- Wilson, J. W., & Roberts, R. D. (2006). Summary of convective storm initiation and evolution during IHOP: Observational and modeling perspective. *Monthly Weather Review*, 134(1), 23–47. <https://doi.org/10.1175/mwr3069.1>
- Wilson, J. W., & Schreiber, W. E. (1986). Initiation of convective storms at radar-observed boundary-layer convergence lines. *Monthly Weather Review*, 114(12), 2516–2536. [https://doi.org/10.1175/1520-0493\(1986\)114<2516:iocksar>2.0.co;2](https://doi.org/10.1175/1520-0493(1986)114<2516:iocksar>2.0.co;2)
- Xiao, H., Wan, Q. L., Liu, X. T., Zheng, T. F., Feng, L., Xia, F., & Chen, J. H. (2019). Numerical prediction of an extreme rainstorm over the Pearl River Delta region on 7 May 2017 based on WRF-ENKF. *Journal of Tropical Meteorology*, 25(3), 312–323.
- Yang, Y., Ji, X., Zhang, S., Zhu, H., Zheng, P., & Yang, J. (2018). Automatic identification of precipitation cloud based on radar reflectivity area spectrum. *Journal of Applied Meteorological Science*, 29(6), 690–700.
- Yussouf, N., & Stensrud, D. J. (2010). Impact of phased-array radar observations over a short assimilation period: Observing system simulation experiments using an ensemble Kalman filter. *Monthly Weather Review*, 138(2), 517–538. <https://doi.org/10.1175/2009mwr2925.1>
- Zhang, F., Weng, Y., Sippel, J. A., Meng, Z., & Bishop, C. H. (2009). Cloud-resolving hurricane initialization and prediction through assimilation of Doppler radar observations with an ensemble Kalman filter. *Monthly Weather Review*, 137(7), 2105–2125.
- Zhang, F. Q., Snyder, C., & Sun, J. Z. (2004). Impacts of initial estimate and observation availability on convective-scale data assimilation with an ensemble Kalman filter. *Monthly Weather Review*, 132(5), 1238–1253. [https://doi.org/10.1175/1520-0493\(2004\)132<1238:ioieao>2.0.co;2](https://doi.org/10.1175/1520-0493(2004)132<1238:ioieao>2.0.co;2)
- Zhang, X., Huang, X., Liu, X. A., Lu, J., Geng, L., Huang, H., & Zhen, G. (2022). The hazardous convective storm monitoring of phased-array antenna radar at Daxing International Airport of Beijing. *Journal of Applied Meteorological Science*, 33(2), 192–204.

- Zhou, A., Zhao, K., Lee, W. C., Ding, Z. C., Lu, Y. H., & Huang, H. (2022). Evaluation and modification of microphysics schemes on the cold pool evolution for a simulated bow echo in Southeast China. *Journal of Geophysical Research: Atmospheres*, 127, e2021JD035262. <https://doi.org/10.1029/2021JD035262>
- Zhu, L., Wan, Q. L., Shen, X. Y., Meng, Z. Y., Zhang, F. Q., Weng, Y. H., et al. (2016). Prediction and predictability of high-impact western pacific landfalling tropical cyclone Vicente (2012) through convection-permitting ensemble assimilation of Doppler radar velocity. *Monthly Weather Review*, 144(1), 21–43. <https://doi.org/10.1175/mwr-d-14-00403.1>
- Zrnic, D. S., Kimpel, J. F., Forsyth, D. E., Shapiro, A., Crain, G., Ferek, R., et al. (2007). Agile-beam phased array radar for weather observations. *Bulletin of the American Meteorological Society*, 88(11), 1753–1766. <https://doi.org/10.1175/bams-88-11-1753>